# Analytical Magnetic Field and Driving Force Models based on Measured Boundary Conditions for Industrial Coriolis Mass Flowmeters

**Li-Jun Wang, Liang Hu, Kok-Meng Lee,** *IEEE Fellow*, **Xiao-Dong Ruan** and **Xin Fu**

***Abstract* – Coriolis mass flowmeters (CMFs) have been widely used in industry because of its high precision (up to 0.1% on flow rig). A precondition to ensure the excellent performance of a CMF is that its measuring tube must vibrate with proper amplitude under different operating conditions. It is thus necessary to modify the driving force of its electromagnetic actuator (EMA), which however cannot be measured directly by means of a traditional force sensor. This paper presents an analytical model for calculating the EMA force of a CMF providing a means to predict some parametric effects on its performance. Specifically, the analytical model of a curved-tube CMF has been derived in closed forms for reconstructing the magnetic field from measured boundary conditions, and for calculating the Lorentz force of a permanent-magnet (PM) based EMA in this paper. This novel coupled measurement-calculation approach, which relaxes the assumption of known magnetic property of the PM, has been validated through a series of experiments, and applied to actual CMF offering insightful findings for designing EMA in CMF applications. Two sets of results are presented. The first set investigates the effect of two different loads on the vibration amplitude. The second set reveals the influence of vibration amplitudes on the Lorentz force of the EMA.**

***Index Terms* –Coriolis mass flowmeter, electromagnetic actuator, driving force, analytical model, magnetic field, reconstruction, Lorentz force**

## I. Introduction

Coriolis mass flowmeters (CMFs) are among the most accurate instruments in industry for measuring mass flowrate[1], where measurements are made by maintaining the vibration of two independent vibrating tubes (VT) with fixed ends [1][2]. Electromagnetic actuators (EMAs) are commonly used in CMF to drive the VT vibration. Owning to its high precision, CMFs are widely used in various industrial and engineering areas, such as measurement of ingredients for quality control of chemical reaction [3] and fuel measurement for an aircraft rocket [4].

To maintain the CMF performance, the driving force provided by the EMA on the tubes must be appropriately modified so that they vibrate with proper amplitude for any operating conditions. Classical proportional plus integral (PI) algorithms are commonly employed to control the vibration amplitude of the measuring tubes, where mapping from driving current to vibration amplitude is included to avoid explicitly determining the EMA driving force [5]. Some recent digital CMFs, adopting PI algorithms, have shown better performance than previous analogue CMFs when measuring fast changing small flows [6], flows batching from empty [7], or two phases (gas-liquid) flows [8][9]. While high signal-to-noise ratio (SNR) for the EMSs can be achieved with large vibration amplitude [10]; the trade-off is the difficulty to maintain stability when dealing with different flow conditions and vibration loads, which significantly influence the accuracy of CMF [11].

Nevertheless, the ability to accurately calculate the EMA forces is highly desirable during the design of a CMF as it offers an essential basis to analyze the effects of the driving current and VT parameters (material, size and shape etc.) on the tube vibration, and hence predict these effects on the operating performance of the CMF. Such findings will help define an appropriate operating current when designing an EMA, and offer some intuitive insights potentially useful to controller design. Taking the specific application in this paper as an example, the value of vibration amplitude (and hence the exciting current passing through the EMA) could be pre-determined based on the analytical force model.

However, as the coil and permanent magnet (PM) of the EMA are separately attached on the two independent tubes [3], it is generally clumsy to mount force sensors on the VTs for measuring the EMA force. In addition, the increase in inertia and reaction forces due to the added sensors will change the VT vibration characteristics and distort the measured EMA force. An alternative approach is to determine the EMA force by means of a calculation method. Numerical methods have been adopted to study the relation between the exciting current, driving force and vibration amplitude for different shaped VT [12]. However, these numerical methods are often

Manuscript received February 1, 2011. Accepted for publication November 3, 2011.



This work was financially supported by the National Basic Research Program (973) of China (No.2011CB013300), Natural Science Foundation of China (No.91023015), Postdoctoral Science Foundation of China (No.20100481416).

L.-J. Wan, L. Hu (corresponding author), X.-.D. Ruan and X. Fu are with the State Key Laboratory of Fluid Power Transmission and Control, Zhejiang University, Hangzhou, China, 310027. (e-mail: dagouwang@zju.edu.cn, cmeehuli@zju.edu.cn, xdruan@zju.edu.cn, and xfu@zju.edu.cn).

K.-M. Lee is with the George W. Woodruff School of Mechanical Engineering, Georgia Institute of Technology, Atlanta, GA 30332-0405 USA (e-mail: kokmeng.lee@me.gatech.edu). He is also visiting Pao Yu-Kong Chair Professor at Zhejiang University,

computation-time costly for real-time applications as moving meshes are required to adapt the vibration between the PM and coils [13]. Therefore, this paper presents an analytical model based on measured boundary conditions for developing a model-based method to determine the EMA forces of a high-precision CMF.

Several methods are commonly employed to calculate forces and torques involved in an electromagnetic devices; namely, Maxwell stress tensor [14], virtual work method [15], Lorentz force law [16] and dipole methods [17][18]. Among these methods, Lorentz force law is especially useful when the force or torque is generated by a current-carrying conductor laying in the magnetic field of PM [18][19][20]; the EMAs of CMF belong to this case. To ensure high-precision calculation of Lorentz force law, the magnetic field distribution of the PM acting on the current-carrying conductor must be accurately determined. Calculating the field based on the remanence property of the PM is a commonly used method [20][21][22]. However, the remanence property is difficult to measure and susceptible to environment effects (such as temperature changes). Accordingly, it is difficult to meet the stringent requirements of high precision CMF using this method. Recently, a reconstruction method has been proposed in [23] to numerically determine the magnetic flux density (MFD) distribution around the PM, and has been applied in spherical motors [23] and electromagnetic flowmeters [24][25]. This method, which relaxes the assumption of known geometry or property of the PM commonly made in other analytical or computational methods, requires only measurement of the normal MFD distribution on the surface of the PM; thus, high precision reconstruction can be achieved.

This paper presents an analytical model based on magnetic field reconstruction for calculating EMA force of a CMF. It is a new application of the reconstruction method. Different from the prior applications where the magnetic fields were reconstructed using finite-element methods, we adopt here an analytical method to reconstruct the field around the PM and calculate the EMA force for design optimization of an electromagnetic CMF. The remainder of this paper offers the followings:

1. The analytical models for reconstructing the PM magnetic field and calculating the Lorentz force of a curved-tube CMF are derived. Given in closed form, the reconstructed magnetic field and force models have been experimentally validated.
2. The models have been applied on a CMF for investigating the effects of different loads on the electromagnetically induced vibration and forces. The intuitive experimental and numerical findings presented here offer some useful insights for guiding the design of a CMF.

## II. Analytical Model of EMA Force

Fig. 1(a) illustrates the structure of a CMF, which consists of two curve-tube VTs, an electromagnetic actuator (EMA) and a pair of electromagnetic sensors (EMS, installed symmetrically at upstream and downstream with EMA respectively). Fig. 1(b) defines the characteristic parameters of the EMA, where the cylindrical coordinate system ($\rho$, $\theta$, $z$) describing the axial (or $z$ direction) motion of the PM is assigned at its geometrical center.

During operation, both tubes vibrate at the same frequency but opposite in phase (with motion perpendicular to the mid plane between the two tubes). With no flow through the VTs (fluid velocity $v$=0m/s), every parts of the single tube vibrates synchronous (in phase). Any existence of the mass flow causes the tubes to twist slightly due to the action of Coriolis force $\mathbf{F_C}$, which exerts a pair of forces equal in magnitude (linearly proportional to the mass flow velocity) but opposite in direction at the upstream and downstream "arms" of the tubes. The out-of-plane twisting causes the upstream arm to lag behind and the downstream arm to lead ahead in the vibratory motion. The out-of-sync phase shift is a measure for the amount of mass flowing through the tubes, and is monitored by the pair of EMSs (installed at upstream and downstream as shown in Fig. 1(a)) which output voltage signals proportional to the local vibration velocities. The motions measured by the EMS pair are contributed by the two forces; Coriolis force $\mathbf{F_C}$ and Lorentz force $\mathbf{F}$. The latter generated by the EMA can be adjusted to compensate for changes in operating conditions if the magnetic field (and hence the Lorentz force) can be accurately determined.

The magnetic force of the EMA acting on the tubes can be calculated from the Lorentz force law [16] with the aid of Fig. 2(a). The current $I$ flows through a differential cross-sectional area d$s$=d$\rho$d$z$ can be written as $J$(d$\rho$d$z$), where $J$ is the current density. From the Lorentz force law, the differential force exerted on a differential length segment (d$\mathbf{l}$=$\rho$d$\theta\mathbf{e}_\theta$ where $\mathbf{e}_\theta$ denotes the unit vector in the $\theta$ direction) of the current carrying conductor in the external magnetic field $\mathbf{B}$ is given by (1):

$$\mathrm{d}\mathbf{F} = \left(J\mathrm{d}\rho\mathrm{d}z\right)\left(\rho\mathrm{d}\theta\mathbf{e}_\theta\right)\times\mathbf{B} \tag{1}$$

Only $B_\rho\mathbf{e}_\rho$ (orthogonal to the direction of the current flowing in the coil) is required in the calculation of (1) due to $\mathbf{e}_\theta\times\mathbf{e}_\rho=\mathbf{e}_z$, where $\mathbf{e}_\rho$, $\mathbf{e}_\theta$ and $\mathbf{e}_z$ denote the unit vectors in $\rho$, $\theta$ and $z$ directions respectively. Thus, the magnetic force in the $z$ direction can be obtained by integrating (1) over the entire volume covered by the coil ($r_c\le\rho\le r_c+h_c$ and $-(l_c+z_c)\le z\le -z_c$ as shown in Fig. 2(a)):

$$\mathbf{F} = -2\pi J\int_{-l_c+z_c}^{z_c}\int_{r_c}^{r_c+h_c} B_\rho(\rho,z)\rho\mathrm{d}\rho\mathrm{d}z\mathbf{e}_z \tag{2}$$

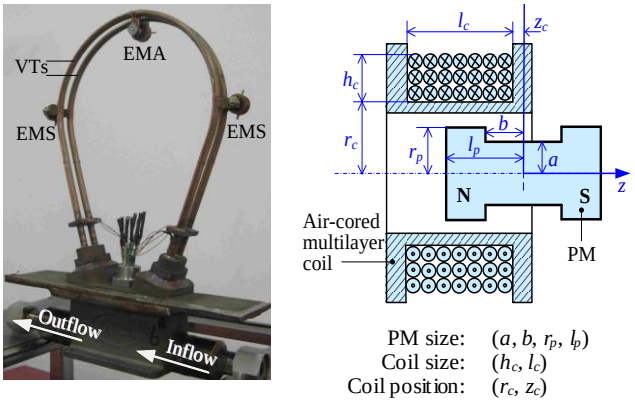


(a) Curved-tube CMF (b) Illustration of the EMA

Fig.1 CMF with double curved-tubes

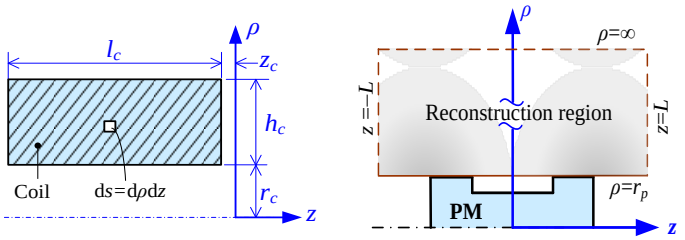


(a) Integral region of force (b) Reconstruction region of magnetic field

Fig. 2 Computational regions for force and potential field

Magnetic field reconstruction of PM

Precise calculation of the Lorentz force relies on accurate $B_\rho(\rho,z)$ distribution. For this, a closed-form analytic solution, which solve the Laplace's equation using the separation of variables, is derived to reconstruct the $B_\rho(\rho,z)$ distribution from measured boundary conditions.

Lorentz force calculation only requires the magnetic field distribution $B_\rho(\rho,z)$ in the region covering the coil, i.e., $[r_p \le \rho \le \infty, -L \le z \le L]$ defined in Fig. 2(b). Here, $L >> l_c$ is set to ensure the field strength is negligible as long as beyond the boundary $z=\pm L$. In the absence of the coil, the region around the PM is current-free (**J**=0) where the magnetic field can be characterized by a Laplace's equation $\nabla^2\psi = 0$. The scalar magnetic potential $\psi$ is defined in (3):

$$\mathbf{B} = \mu\mathbf{H} = -\mu\nabla\psi \tag{3}$$

where $\mu$ is the magnetic permeability of the material (air) in the reconstruction region. In cylindrical coordinates, the Laplace's equation (with the assumption that $\partial\psi/\partial\theta$=0) and boundary conditions for the EMA are given in (4):

$$\frac{1}{\rho}\frac{\partial}{\partial\rho}\left(\rho\frac{\partial\psi}{\partial\rho}\right)+\frac{\partial^2\psi}{\partial z^2}=0 \tag{4}$$

$$-L \le z \le L \qquad \partial\psi/\partial\rho\big|_{\rho=r_p} = -\left[B_\rho(z)/\mu\right]\big|_{\rho=r_p}, \qquad \psi\big|_{\rho=\infty}=0 \tag{4a,b}$$

$$r \le \rho \le \infty \qquad \partial\psi/\partial z\big|_{z=\pm L}=0 \tag{4c}$$

The Neumann boundary condition (NBC) in (4a) specifies the normal magnetic flux density at the boundary $\rho=r_p$. The Dirichlet boundary condition (DBC) in (4b) and the NBC in (4c) assume that the infinitely far field and the normal magnetic flux density passing through the boundaries $z=\pm L$ are negligible.

Based on the separation of variables, the general solution to the Laplace's equation has the following form:

$$\psi(\rho,z)=\sum_{m=1}^{\infty}\begin{bmatrix}A_m\cos(\omega_m z)\\ B_m\sin(\omega_m z)\end{bmatrix}\begin{bmatrix}C_m I_0(\omega_m\rho)+\\ D_m K_0(\omega_m\rho)\end{bmatrix} \tag{5}$$

where the two square brackets are the general solutions for the independent functions $Z(z)$ and $R(\rho)$ respectively; $I_0(\omega_m\rho)$ and $K_0(\omega_m\rho)$ are zero-order modified Bessel functions of first and second kinds; and $A_m$, $B_m$, $C_m$, $D_m$ and $\omega_m$ are the coefficients to be determined from the BCs (4a-c).

The odd symmetry of the field about the $z$ axis implies that $\cos(\omega_m z)$ must be omitted, and hence $A_m$ =0. Since $I_0(\omega_m\rho)\to\infty$ as $\rho\to\infty$, this, together with the DBC (4b), further implies that $C_m$ =0. From the homogeneous NBC (4c), we have

$$\omega_m = \frac{m\pi}{2L},\ m=2k+1,\ k=0,\ 1,\ 2,\ \ldots \tag{6}$$

Thus, the general solution (5) reduces to (7) with the unknown coefficient $\xi_m=B_mD_m$ to be determined form the NBC (4a):

$$\psi(\rho,z)=\sum_{\substack{k=0\\ m=2k+1}}^{\infty}\xi_m\sin\left(\frac{m\pi}{2L}z\right)K_0\left(\frac{m\pi}{2L}\rho\right) \tag{7}$$

Noting the orthogonal characteristics of the sine function,

$$\int_{-L}^{L}\sin\left(\frac{m\pi}{2L}z\right)\sin\left(\frac{n\pi}{2L}z\right)dz=\begin{cases}L & m=n\\ 0 & m\ne n\end{cases}$$

$$\xi_m=-\frac{\int_{-L}^{L}B_\rho(z)\big|_{\rho=r_p}\sin(\omega_m z)\,\mathrm{d}z}{\mu L\omega_m K_0'(\omega_m r_p)} \tag{8}$$

where $K_0'(\omega_m r_p)$ is the derivative of the zero-order virtual Bessel function of second kind; and $K_0'(x)=-K_1(x)$.

Using (3) and (7), the magnetic flux density distribution in the $\rho$ direction can be computed from (9):

$$\mathbf{B}=\begin{bmatrix}B_\rho(\rho,z)\\ B_z(\rho,z)\end{bmatrix}=\begin{bmatrix}\mu\sum\limits_{\substack{k=0\\ m=2k+1}}^{\infty}\xi_m\omega_m\sin(\omega_m z)K_1(\omega_m\rho)\\ -\mu\sum\limits_{\substack{k=0\\ m=2k+1}}^{\infty}\xi_m\omega_m\cos(\omega_m z)K_0(\omega_m\rho)\end{bmatrix} \tag{9}$$

where $\omega_m$ and $\xi_m$ are given in (6) and (8) respectively. Only the radial component $B_\rho$ is required in the calculation of the Lorentz force. $B_z$ is given here for completeness. It is also worth noting that no detailed PM geometry is required in reconstructing **B**.

Closed-form Lorentz force equation

Once $B_\rho\left(\rho=r_p,-L\le z\le L\right)$ in the DNC (4a) is measured, the $B_\rho$ distribution can be determined from (9). For a specified coil (geometry and position) of the EMA, the Lorentz force can be calculated from the integral from (2) leading to (10):

$$\mathbf{F}(J,z_c)=\frac{S\mu J\pi r_c^2}{2}\left[H_c^2 G_{1\,3}^{2\,1}\left(\frac{v_m H_c}{2},\frac{1}{2}\Big|_{-\frac{1}{2}\ \frac{1}{2}\ -1}^{0}\right)-G_{1\,3}^{2\,1}\left(\frac{v_m}{2},\frac{1}{2}\Big|_{-\frac{1}{2}\ \frac{1}{2}\ -1}^{0}\right)\right] \tag{10}$$

where $$S=\sum_{\substack{k=0\\ m=2k+1}}^{\infty}\xi_m\left(\cos\left[\omega_m\left(l_c-z_c\right)\right]-\cos(\omega_m z_c)\right)$$

$$H_c=1+\frac{h_c}{r_c} \qquad \text{and} \qquad v_m=\omega_m r_c$$

In (10), the Meijer G-function is evaluated as a hyper-geometric series of gamma function Ã in (11):

$$G_{p\,q}^{m\,n}\left(x,r\Big|_{b_1,\ \ldots,\ b_q}^{a_1,\ \ldots,\ a_p}\right)=\frac{1}{2\pi i}\int_{\mathrm{T}}\frac{\prod_{j=1}^{m}\Gamma(b_j+s)\prod_{j=1}^{n}\Gamma(1-a_j-s)}{\prod_{j=n+1}^{p}\Gamma(a_j+s)\prod_{j=m+1}^{q}\Gamma(1-b_j-s)}\cdot x^{-s/r}ds \tag{11}$$

where the gamma function Γ and contour T are set up to lie between the poles of $\Gamma(1-a_j-s)$ and those of $\Gamma(b_j+s)$ [26]. Although the Meijer function in Eq. (10) and (11) cannot be reduced to a simple analytical expression, the function can be conveniently calculated using off-the-shelf software (such as Matlab and Mathematica, which have specific functions to solve this problem). Since the parameters, $r_c$ and $h_c$, are given constants for an actual CMF, the values of the Meijer G-function can be pre-calculated (and stored as look-up table) for use directly in actual force computation. As shown in (10), the Lorentz force is linearly proportional to the current through the coil but a non-linear function of the relative position $z_c$ between

the PM and coil. This relative position $z_c$ is a net effect of both Coriolis and Lorentz forces.

In practice, table look-up methods can be used to obtain the parametric values needed in the model, such as the $G$ function in (11) and $\xi_m$ in (8). Furthermore, the required terms to calculate the force according to equation (11) will not exceed 30. Thus, the force calculation can be completed in about 1ms, significantly shorter than the vibration period of a CMF (typically in the range of 80 to 100 Hz) by an order of magnitude.

Electromagnetically induced vibration

With the closed-form solution (10), the position-dependent Lorentz force can be explicitly calculated for simulating the VT vibration using a FE model. According to [12], the governing equations of the FE model can be derived by Hamilton's variation principle as follows:

$$\int_{t_1}^{t_2} \delta(W_p - W_k)dt = 0 \tag{12}$$

In (12), the total potential energy $W_p$ and kinetic energy $W_k$ of the moving solid structure given by the integrals (13) and (14):

$$W_p = \frac{1}{2}\int_{\Omega_s} \sigma_s : \varepsilon_s d\Omega - \int_{\Gamma_s} p_s . u_s d\Gamma - F.r_p \tag{13}$$

$$W_k = \frac{1}{2}\int_{\Omega_s} \rho_s(\mathbf{V_s}\cdot\mathbf{V_s})d\Omega \tag{14}$$

where $\Omega_s$ and $\Gamma_s$ denote the domain and its boundary of the VT structure with velocity field $\mathbf{V_s}$; $\varepsilon_s$ and $\sigma_s$ are the strain and the stress tensors in the structure respectively; $p_s$ is the surface tractions acting upon the moving boundary through the respective displacement field $u_s$; $\mathbf{F}$ is the EMA force applied at the driving point; and $\mathbf{r}_p$ is the position vector describing the driving point; and $\rho_s$ is the density of the structure material.
with the initial and boundary conditions as follows:

$$\begin{aligned} &u_s(x,t) = 0, x \in \Gamma \\ &\sigma_s(x,t)\cdot n(x,t) = p_s(x,t), x \in \Gamma(t) \\ &F(t) = (F(t),0,0), x = x_{r_p} \end{aligned} \tag{15}$$

For a given design, Equations (12) to (13) can be formulated and solved using commercial FEM software (such as ANSYS).

## III. Results and Discussion

Experiments were conducted to determine the coefficient $\xi_m$ in (8) and hence the magnetic field (9) and the Lorentz force (10) for the CMF shown in Fig. 1, where the geometrical dimensions of the EMA are listed in Table 1. These experimental studies provide a basis to validate the magnetic field reconstruction around the PM (without the coil) and the force model using the analytical solution with measured boundary conditions. Once the computational results are verified, the force model can be effectively employed to investigate the effect of the relative position $z_c$ on the Lorentz force; both static and time-varying changes in $z_c$ are considered. In typical commercial CMFs, drive currents are generally limited in 100mA; and VT vibration amplitudes do not exceed 1mm. However, for the purpose of experimental validation, the model and drive current are allowed to exceed 100mA (but with a very short duration) during the process of adjusting the vibration amplitude [9][11]. Thus, the test current is limited in 0.25A.

Table. 1 Characteristic values of the EMA (Dimensions in mm)

| PM size | | Coil | | | | | |
|---|---|---|---|---|---|---|---|
| | | Size | | Position | | Ampere-turn | |
| $(r_p, l_p)$ | (7, 9.5) | $h_c$ | 3 | $r_c$ | 10 | $I$ | –0.1 A to 0.1 A |
| $(a, b)$ | (5, 4.3) | $l_c$ | 15 | $z_c$ | –5 to 5 | $N$ | 1100 turns |

### A. Validation of magnetic field reconstruction

For the Lorentz force calculation involved in the CMF, the distribution of the $B_\rho(z)$ required in the NBC (4a) was experimentally determined using a Hall probe (accuracy within ±0.2%) system shown in Fig. 3. The probe, positioned by the computer-controlled scanning servo mechanism and monitored by a gauss meter [23], measures the average value of the normal component of **B** passing through the small Hall-effect area (1mm diameter) located at the end of the probe. To measure in the space taken by the coil along $z$ direction, the PM was mounted on a long non-magnetic holder.

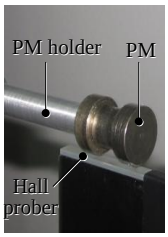


(a) Measurement of $B_n(z)$

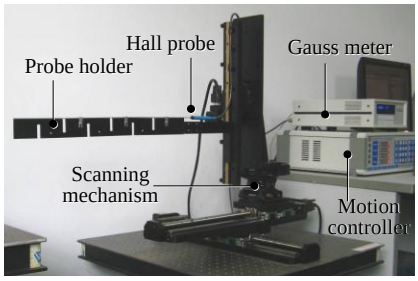


(b) BC measurement setup (adapted from [13])

Fig.3 Experimental setup for measuring $B_\rho$ required in the NBC (4a).

Guided by a motion controller, the servo system (with translational resolution and accuracy of 5μm and 8μm respectively) scanned $B_\rho(z, \rho=r_p=7\text{mm})$ with the hall probe, for which 201 measurements covering the range $|z| \le 100$mm (or 1mm per step). The results are shown in Fig. 4(a); as $B_\rho \to 0$ for $|z| > 50$mm, only data in $|z| \le 50$mm are plotted. Using data in Fig. 4(a), the magnetic field of the PM in the region covered by the coil is computed from (9) and plotted in Fig. 4(b). To verify the reconstructed data experimentally, three additional $B_\rho(z)$ measurements at $\rho=r_c=10$mm, $\rho=r_c+h_c=13$mm, and $\rho=17$mm are given in Fig. 4(a), where the comparisons agree well.

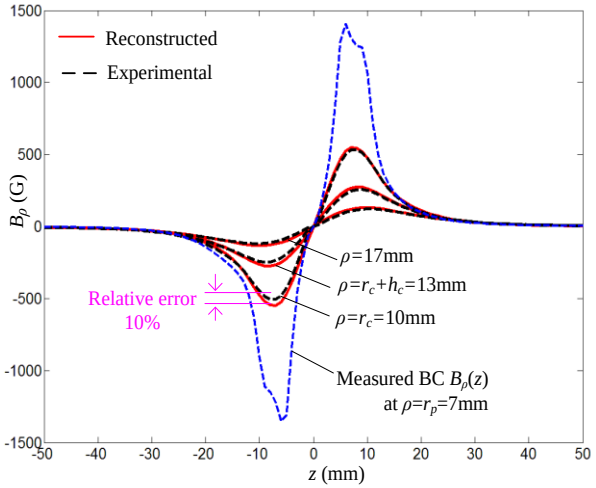


(a) Measured BC, and selected comparison of reconstructed and measured data

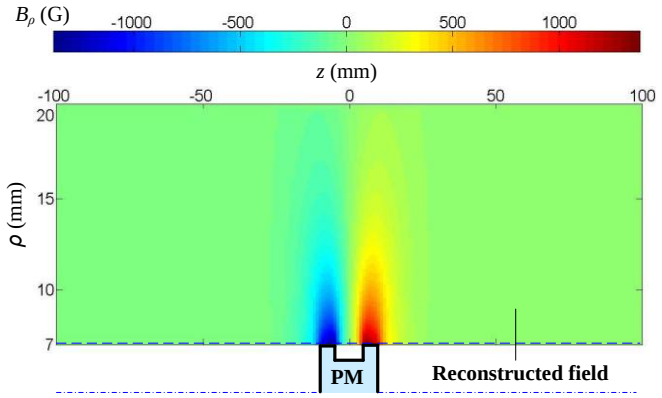


(b) Reconstructed $B_\rho(\rho, z)$ of the PM in region

Fig. 4 $B_\rho(\rho, z)$ of the PM in region [7mm $\le \rho \le$ 20mm, -100mm $\le z \le$100mm]

### B. *Validation of Lorentz force calculation*

With the $B_\rho$ at the NBC (4a) in Fig. 4(a), the coefficient $\xi_m$ (8) and hence the Lorentz force (10) can be calculated in terms of current $I$ and relative displacement $z_c$ between the PM and the coil of the EMA. The force model has been verified experimentally using the setup shown in Fig. 5, where the EMA force corresponding to different relative positions between the PM and the multilayer coil and different input currents were measured. An adjustable elevating platform (60mm stroke and 0.01mm resolution) provides a means to adjust the relative position $z_c$ between the PM (attached to the elevating platform) and the multilayer coil (installed on the aluminum holder). The $z_c$ is monitored by a laser displacement sensor (LDS). An electronic scale (with 0.5g resolution) is used to measure the force, since the force of this EMA is too small (smaller than 1N as given below) to be measured by traditional force sensors. The PM along with the elevating platform is putting on the scale, then the EMA force can be determined according to the scale reading changing when there is static current passing through the EMA.


Fig. 5 Experiment setup to measure the EMA force

The following cases were computed and compared against experimental measurements in Figs. 6 and 7:

- Lorentz force as a function of the current $I$ at $z_c$=0mm; this relationship is linear as given in (10). The difference between computed and measured forces for the range [0A, 0.25A] is compared in Fig. 6, which shows excellent agreement. The maximum relative error for the range tested is about 3.4%.
- Lorentz force as a function of the relative displacement $z_c$ with $I$=0.1A. Because of the space restriction between the coil and PM, $z_c$ is limited to [-5mm, 5mm] in measurements. The results are compared in Fig. 7. As expected, the force-displacement is nonlinear. The Lorentz force is expected to be zero at $z_c=l_c/2$ =7.5mm since the magnetic field around the PM is an odd symmetry about the z axis. The large gradient of the PM magnetic field (Fig. 4) has an effect of "amplifying" any small geometrical and positioning errors of the coil on the force calculation; this results in some discrepancy between the force model and experimental data as observed in Fig. 7, which otherwise agree very well.

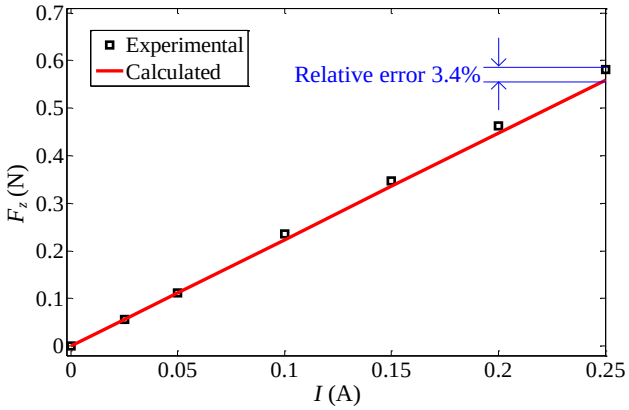


Fig. 6 Comparison of the calculated force against experimentally measured results for different current $I$=0~0.25A at a specified position $z_c$=0mm

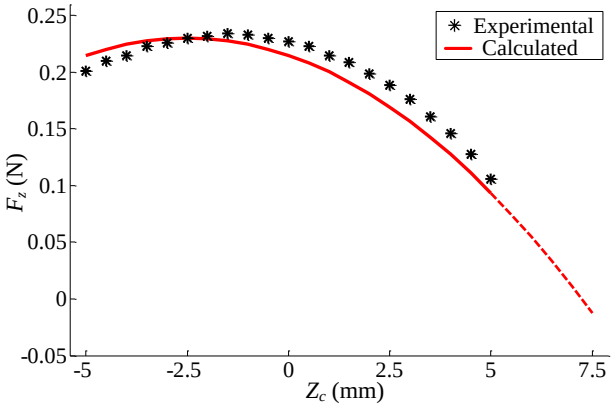


Fig. 7 Comparison between calculated force and measured results, $I$=0.1A

### C. *Effects of vibration amplitudes on Lorentz force*

Fig. 8(a) shows the FE model for the curved-tubes of the CMF in Fig. 1 with the experimental setup given Fig. 8(b). Since the two tubes have the almost same vibration magnitude, only one tube (rigidly connected at both ends) is modeled in the calculation. The fluid in VT is treated as a vibration load; and both the EMA and EMSs are also considered as added masses. The deformation caused by the vibration is small enough; thus the linear elastic theory is adopted in this FE model. The vibration displacement between the PM and the coil of the EMA was measured in real time using two high-precision laser displacement sensors (LDS), with 0.05μm resolution and 20ns response time.

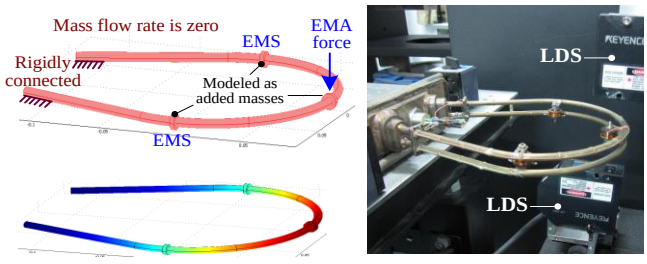


(a) FE model (b) Experiment setup

Fig.8 FE model and experiment set up to calculate and measure the VT vibration

Two sets of results are presented here. The 1st set investigates (experimentally and analytically) the effect of vibration load on the displacement of VT vibration. The VTs were filled with two different fluids, kerosene and water, for simulating different loads. In the experiment, the tubes are open-loop driven by sinusoidal currents with same amplitude from a signal source; and both tubes vibrate at their fundamental frequency respectively. To isolate the Lorentz force from the Coriolis effects, the flowrate through the VT was kept at zero. Computed vibration displacements are compared against experimental results in Fig.9, where the small differences between the calculated and measured data well validate the method presented in this paper. In addition, kerosene has a lighter density than water and thus, there is a small difference between the fundamental frequencies corresponding to the two loads. Even though the tubes are driven by an amplitude-fixed current (50mA) at their fundamental frequency respectively, an accompanied difference about 6% in the vibration amplitude can still be observed in Fig. 9. This difference implies that the CMF is sensitive to the vibration load and thus the exciting current must be changed accordingly to maintain the designed amplitude. As current is often limited due to drive power saturation for a given design, appropriate vibration amplitude must be pre-defined when designing a CMF based on the drive capability and potential load conditions.

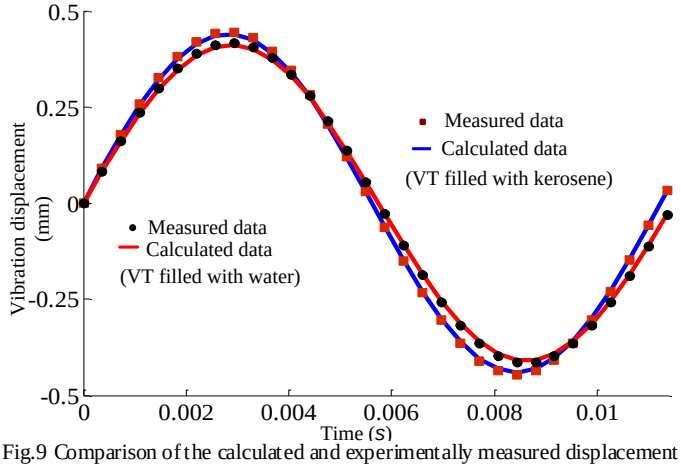


Fig.9 Comparison of the calculated and experimentally measured displacement

The 2nd set numerically examines the influences of vibration amplitudes on the Lorentz force depending on the relative displacement $z_c$ given in (2), where reconstructed magnetic field data in the region $[r_c \le \rho \le r_c+h_c,\ -l_c-z_c \le z \le -z_c]$ are required to calculate the Lorentz force during vibration. In this numerical examine, a sinusoidal drive current with fixed amplitude (which ensure EMA force with the same amplitude) is supposed to pass through three EMAs fixed on different tubes. Correspondingly, three tubes will show vibrations with different amplitude, and then their influence on the EMA force is examined in this set. Fig. 10(a) shows the computed response of the Lorentz force (normalized to its amplitude) to a same sinusoidal input current but with three different vibration amplitudes (VA) , 0.25, 0.75 and 1.25 mm. As the vibration amplitude increases, harmonic distortion on the Lorentz force becomes more and more noticeable as shown in Fig. 10(a) where the differences of $F_z$ (normalized to its amplitude) from a perfect sine function are compared. This observation has been confirmed by analyzing the corresponding frequency spectrum in Fig. 10(b), which shows the fundamental frequency at about 90Hz and a noticeable harmonic component around 270Hz. Special attention should be pay to this phenomenon, which further confirms that it is reasonable to limit the vibration amplitude under 1mm; while larger vibration amplitude may bring better signal-to-noise ratio (SNR) for the EMS, the trade-off is the increased losses due to harmonic distortion.

## IV. CONCLUSIONS

An analytical model to calculate the driving force of the EMA for a CMF has been presented. Different from other force calculation methods, the model employs a coupled measurement/calculation approach (that relaxes the assumption of knowing property of the PM) to reconstruct the magnetic field around the PM from its measured boundary conditions for calculating the Lorentz force of the EMA that drives the vibration. The model which provides a basis for design of a CMF has been experimentally validated by comparing the calculated results against measured data (which agree within a maximum relative error of about 3.4%). The findings in this paper have offered some insightful insights useful for improving the design of a CMF, particularly tradeoff between the vibration amplitude for better SNR and the tolerance to energy losses due to harmonic distortion. Some other applications are also possible based on the precise determining of the EMA force, such as real-time evaluation of tube dampings which is closely related to the CMF performance.

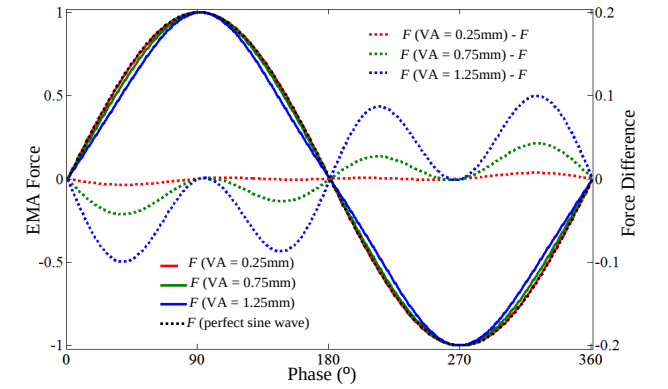


(a) Time domain waveform (normalized)

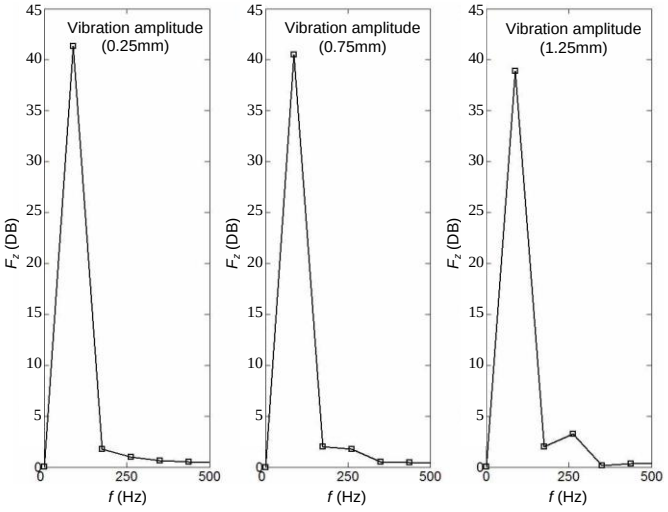


(b) Spectrum obtained by FFT

Fig.10 The non-sinusoid of the EMA force as the vibration amplitude of the VT becomes more and more large

## REFERENCES


[1] M. Anklin, W. Drahm, Alfred Rieder. "Coriolis mass flowmeters: Overview of the current state of the art and latest research," *Flow Meas. and Instrum*., 17, (2006), 317-323.

[2] R. Smith, D. R. Sparks, D. Riley, N. Najafi. "A MEMS-Based Coriolis Mass Flow Sensor for Industrial Applications," *IEEE Trans. on Ind. Electron*, Vol. 56, No.4, 2009.

[3] Baker RC. "Coriolis flowmeters: Industrial practice and published information," *Flow Meas. and Instrum*, 5(4), (1994), 229-46.

[4] Furio Cascetta, Giuseppe Rotondo, Marilena Musto. "Measuring of compressed natural gas in automotive application: A comparative analysis of mass versus volumetric metering methods," *Flow Meas. and Instrum.*, 19, (2008), 339-341.

[5] D. W. Clarke. "Nonlinear control of oscillation amplitude of a Coriolis mass flow meter," *Eur. J. Contro*l, 4, (1998), 196-207.

[6] C. Clark, M. Zamora, R. Cheesewright, and M. Henry. The dynamic performance of a new ultra-fast response Coriolis flow meter. *Flow Meas. Instrum*., vol. 17, no.6, pp.391-398, Dec. 2006.

[7] M. P. Henry. "Breakthrough-Coriolis meter allows filling machine to operate with exceptional precision," *Control Eng. Eur.*, vol. 5, no. 3, pp. 8-9, Jun. 2004.

[8] M. Henry, H. Yeung, W. Mattar, M. Duta, and M. Tombs. How a Coriolis mass flow meter can operate in two phase (gas/liquid) flow. Presented at the ISA, Houston, TX, 2004.

[9] Mayela Zamora, Manus P. Henry. "An FPGA Implementation of a Digital Coriolis Mass Flow Metering Drive System", *IEEE Trans. on Ind. Electron*., Vol. 55, No.7, 2008.

[10] Robert Cheesewright, Ali Belhadj, Colin Clark. "Effect of Mechanical Vibrations on Coriolis Mass Flow Meters," *J. of Dyn. Sys. Meas. and Control*, 125, (2003), 103-113.

[11] M. P. Henry, D. W. Clarke, N. Archer, J. Bowles, M. J. Leahy, R. P. Liu, J. Vignos, and F. B. Zhou. "A self-validating digital Coriolis mass flow meter: An overview," *Control Eng. Pract.*, 8, (2000), 487-506.

[12] N. Mole, G. Bobovnik, J. Kutin, B. Stok, I. Bajsic. "An improved three-dimensional coupled fluid-structure model for Coriolis flowmeters," *J. of Fluids and Structures*, 24, (2008), 559-575.

[13] N Sadowski, Y Lefevre, M Lajoie-Mazenc, J Cros. "Finite element torque calculation in electrical machines while considering the movement," *IEEE Trans. on Magnetics*, 28, (2002), 1410-1413.

[14] Wu Dezheng, S. D. Pekarek, B. Fahimi. "A Voltage-Input-Based Field Reconstruction Technique for Efficient Modeling of the Fields and Forces Within Induction Machines," *IEEE Trans. on Ind. Electron*, 57(3), (2010), 994-1001.

[15] T Tarnhuvud, K Reichert. "Accuracy problems of force and torque calculation in FE-systems," *IEEE Trans. on Magnetics*, 24, (2002), 443-446.

[16] Kapjin Lee, Chulsoo Kim, Kyihwan Park. "Development of an eddy-current-type magnetic floor hinge," *IEEE Trans. on Ind. Electron*, 53(2), (2006), 561-568.

[17] K.-M. Lee, K. Bai, and J. Lim, "Dipole Models for Forward/Inverse Torque Computation of Spherical Motor," *IEEE/ASME Trans. on Mechatronics*, vol 14, no. 1, (2009) pp 46-54.

[18] K. C. Lim, L. Yan, I.-M. Chen, G. L. Yang, W. Lin and K. M. Lee, "Electromechanical Modeling of a Permanent Magnet Spherical Actuator based on Magnetic Dipole Moment Principle*," IEEE Trans. on Ind. Electron*.,Vol 56, no. 5, pp. 1640-1648, May 2009.

[19] Julius Adams Stratton. "Electromagnetic Theory," *IEEE Press*, Published by John Wiley & Sons, Inc, 2007.

[20] Yan L, Chen I M, Lim C K, Yang G, Lin W, Lee K M. "Design and analysis of a permanent magnet spherical actuator," *IEEE/ASME Trans. on Mechatronics*, 2008, 13(3):239-248.

[21] H. Son and K.-M. Lee, "Open-loop Controller Design and Dynamic Characteristics of a Spherical Wheel Motor," *IEEE Trans. on Ind. Electron*. (2010),Vol. 57, no. 10, 3475-3482

[22] Lee, K.-M. and H. Son, "Distributed Multipole Model for Design of Permanent-Magnet based Actuators," *IEEE Trans. on Magnetic*, (2007) vol. 43, No. 10, 3904-3913.

[23] L. Hu, K. M. Lee, X. Fu. "A method based on measured boundary conditions for reconstructing the magnetic field distribution of an electromagnetic mechatronic system," *IEEE/ASME Trans. on Mechatronics*, (2010), Vol. 15, No 4, pp 595-602.

[24] L. Hu, J. Zou, X. Fu, H. Y. Yang, X. D. Ruan, C. Y. Wang. "A reconstruction approach to determine the magnetic field around an electromagnetic velocity probe," *Meas. Sci. and Technology*, 2009, 20(1):015-103.

[25] X. Fu, L. Hu, J. Zou, H. Y. Yang, X. D. Ruan, C. Y. Wang. "Divisionally analytical reconstruction of the magnetic field around an electromagnetic velocity probe," *Sensors & Actuators: A. Physical*, 2009, 150(1): 12-23.

[26] Z. L. Xu. "Modern Mathematics Handbook-Classical Mathematics, 1st ed.," *Huazhong University of Science and Technology Press*, Wuhan, China, 2000.


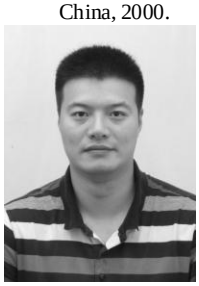

**Li-Jun Wang** received the B.Eng. degree from the Department of Mechanical Engineering, Zhejiang University, Hangzhou, China, in 2008. He is studying for the Ph.D degree now in this department. His current research interests include flow measurement and instrumentation.

**Liang Hu** received the B.Eng. degree from the Department of Mechanical Engineering, Zhejiang University, Hangzhou, China, in 2004, and he also received the Ph.D degree from this department in 2010. His current research interests include flow measurement and instrumentation, measurement and calculation of magnetic field.

**Kok-Meng Lee** (M'89–SM'02–F'05) received the B.S. degree from the State University of New York, Buffalo, in 1980, and the S.M. and Ph.D. degrees from Massachusetts Institute of Technology, Cambridge, in 1982 and 1985, respectively.

He is currently a Professor in the Woodruff School of Mechanical Engineering, Georgia Institute of Technology, Atlanta. His current research interests include system dynamics/control, robotics, automation, and mechatronics. He holds eight patents in machine vision, 3-DOF spherical motor/encoder and live-bird handling system.

Prof. Lee is a Fellow of the American Society of Mechanical Engineers. He received the National Science Foundation Presidential Young Investigator Award, the Sigma Xi Junior Faculty Research Award, the International Hall of Fame New Technology Award, and the Kayamori Best Paper Award.

**Xiao-Dong Ruan** received the B.S. degree from the Department of Mechanical Engineering, Zhejiang University, Hangzhou, China, in 1989, and she also received the M.S. degree from this department in 1992. She received the Ph.D. degree from the Department of Mechanical Engineering, Fukui University, Japan, in 2001.

She is currently a Professor at the Department of Mechanical Engineering, Zhejiang University, Hangzhou, China. Her current research interests include micro-fluidic technology, simulation and visualization of flow field, fluid vibration and noise control, and flow measurement and instrumentation.

**Xin Fu** received the B.Eng. degree from Chengdu University of Science and Technology, Chengdu, China, in 1982, the M.Eng. degree from Southwest Agricultural University, Chongqing, China, in 1990, and the Ph.D degree from University of Leoben, Austria, in 1999.

He is currently a Professor at the Department of Mechanical Engineering, Zhejiang University, Hangzhou, China, where he made research since 1999. His current research interests include micro-fluidic technology, simulation and visualization of flow field, fluid vibration and noise control, and flow measurement and instrumentation.

Dr. Fu was the Director of the State Key Lab of Fluid Power Transmission and Control, China, from 2005 to 2009. Now he is the Vice-Dean of the Department of Mechanical Engineering, Zhejiang University, China.